



Effect of Spin Speed on the Physical Characteristics of CuO Films Synthesized by Sol–Gel Spin Coating for H₂S Gas Sensing

Jyoti¹ · Rajesh Kumar¹

Received: 18 March 2024 / Accepted: 26 August 2024
© The Minerals, Metals & Materials Society 2024

Abstract

In this paper, we study the effects of spinning speed on the electrical, optical, structural, morphological, and gas sensing properties of thin films deposited on glass substrates by sol–gel spin coating, using copper acetate dihydrate as the precursor. The deposition of the films was carried out at varying spinning speeds from 1500 rpm to 2500 rpm to achieve different thicknesses ranging from 157 nm to 470 nm, respectively. The results revealed that the resistivity of the films decreased from 75.5 Ω -m to 42.5 Ω -m with the decrease in spinning speed. X-ray diffraction (XRD) studies demonstrated that the crystallite size varied in the range of 18.14–27.48 nm. The band gap of the samples was found to vary from 2 eV to 1.69 eV, revealing that these samples were suitable for gas sensing applications. Field-emission scanning microscopy (FESEM) studies showed that the prepared samples were porous in nature and were suitable for H₂S gas detection. The films were examined at different operating temperatures with different concentrations of H₂S gas. The results showed that the response toward hydrogen sulfide gas varied with varying thickness of the samples. The CuO thin films showed the highest response toward hydrogen sulfide gas at a temperature of 25°C.

Keywords Thin films · sol–gel spin coating · XRD · UV spectroscopy · H₂S gas · sensor

Introduction

Gas sensors synthesized from metal oxide semiconductors respond to a broad range of oxidizing and reducing gases.^{1,2} Metal oxide-based gas sensors respond to various gases by producing a change in conductivity. These sensors have become popular because of their low cost, portability, compatibility, and small size.^{3–5} However, despite the considerable research over the past few decades on single-metal oxides as semiconductor gas-sensing materials, issues remain because of their high operating temperature, poor selectivity, and inability to detect very low concentrations of gas effectively.⁶ Researchers have proposed various solutions to address these problems. For example, a heterojunction core–shell *p*-CuO/*n*-SnO₂ nanowire (NW)-based sensor was reported with superior selectivity and sensitivity.⁷ Many gases are produced as a result of the modern human lifestyle

and rapid industrial development, resulting in environmental pollution.

Among these gases, H₂S is an extremely toxic gas which is produced by both natural and artificial means. Major sources of H₂S in the environment include petroleum refineries, coal, water sewage, and decay of organic compounds.⁸ Industrial equipment is also affected by hydrogen sulfide because of the acidic solution formed upon dissolving H₂S in water.^{9,10} This gas is highly flammable, with a rotten egg smell, causing environmental pollution and adverse effects on human health. Therefore, a highly sensitive, affordable, and portable sensor is needed for the low-concentration detection of harmful and hazardous H₂S gas. This type of sensor is among the most promising strategies for reducing environmental pollution and overcoming limitations on the use of complex instruments.

The various gas sensors synthesized by both *p*- and *n*-type metal oxides include V₂O₅,¹¹ CeO₂,¹² ZnO,¹³ In₂O₃,¹⁴ SnO₂,¹⁵ WO₃,¹⁶ and NiO.¹⁷ Gas sensors fabricated from films of tin oxide for detecting H₂S gas have demonstrated low sensitivity.¹⁸ CuO thin films can be used as gas sensors to achieve high sensitivity at room temperature, and the response of these films toward H₂S gas is highly reversible.¹⁹

✉ Jyoti
jyotishoran1r3@gmail.com

¹ Department of Physics, Lovely Professional University, Phagwara, Punjab 144411, India

Several nanostructures²⁰ and microstructures²¹ of CuO have been proposed to increase sensing performance. Among these nanostructures, CuO is a *p*-type semiconductor with a band gap lying between 1.2 eV and 2 eV. The gas sensing response can be easily achieved by measuring the change in resistance on exposure to the gas. In addition to several semiconductors, copper oxide exhibits a wide surface area that provides good sensing performance, high surface energy, and good structural and optical properties.

The purpose of this study is to synthesize CuO thin films for application as H₂S gas sensing elements. A two-probe setup and ultraviolet–visible spectroscopy were used to investigate the electrical and optical properties of the CuO thin films, respectively. X-ray diffraction (XRD) and field-emission scanning electron microscopy (FESEM) were used to analyze the structural and morphological properties of samples, respectively. The sol–gel spin coating process was successfully used to create CuO thin films at a concentration of 0.75 M. The gas sensing performance of the synthesized films was studied for different gas concentrations at several operating temperatures. The response curve of the gas sensing elements indicates that the maximum response was achieved around 25°C. The tested samples indicate that for 40 ppm H₂S at 25°C, the maximum sensitivity is 87 and the minimum response time is 20 s.

Experimental

To prepare the precursor solution, copper acetate dihydrate (Cu (CO₂CH₃)₂·2H₂O) was dissolved in isopropanol ((CH₃)₂CHOH). This mixture was stirred for 15 min on a hot plate with a magnetic stirrer in a closed vessel for

initial dissolution. The mixture was then stirred once more for 15 min after the addition of 0.5 ml of diethanolamine (C₄H₁₁NO₂). Lastly, 0.5 ml of polyethylene glycol HO(C₂H₄O)_n was added to the solution and the mixture was stirred continuously for 30 min. All of these chemicals were acquired from Sigma Aldrich, India. Finally, a transparent dark blue solution was obtained. This solution was kept for 12 h to obtain a more stable coating.

For the preparation of thin films, glass slides measuring 2×2 cm were used as substrates. After cleaning the slides, they were dried on a hot plate at 150°C for 10 min. A double-step spinning program (step 1 with 100 rpm spinning speed, 10 s spinning time, 10 s spinning acceleration) was loaded in a spin coater to produce uniform thin films. The solution was deposited at 1500 rpm, 2000 rpm, and 2500 rpm for 30 s to create three thin film samples in the second stage. After depositing the solution, each sample was dried, and this procedure was carried out five times. The samples were finally heated to 400°C for 1 h in a muffle furnace (Fig. 1).

Structural analysis of the thin films was conducted using XRD (Bruker D8 Advance diffractometer) with Cu-K α radiation, scanning from 20° to 80°. Morphological analysis of the prepared samples was carried by FESEM (JEOL JSM-7610F Plus). The optical characteristics of the thin film samples were examined using a Shimadzu UV-1800 spectrophotometer. Electrical characterization of the thin films was performed using a two-probe setup (TPX 200), and fabrication of thin films by a spin coater (SpinNXG-P1). To investigate the gas sensing process, the electrical resistance was measured by pasting two Ag electrodes on the surface of the fabricated CuO thin films. Within the gas chamber, the sensing element was maintained in direct contact with a heater that operated within a temperature range

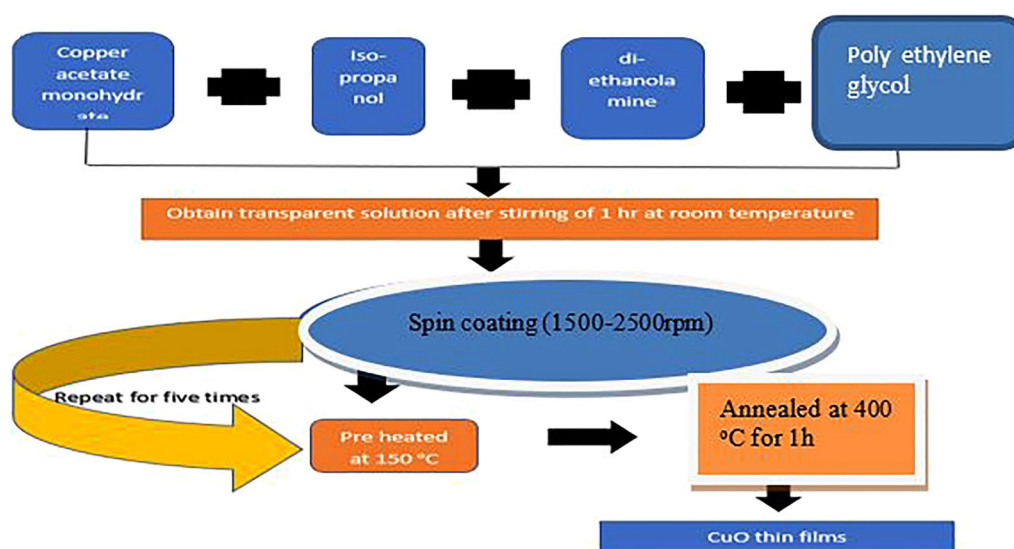


Fig. 1 Procedure for synthesis of thin films.

of 25–100°C. Using a digital picoammeter, the electrical resistance of the sensing element was measured both before and after exposure to H₂S gas.

Results and Discussion

Structural Analysis

The XRD pattern of the deposited CuO films annealed at 400°C for 2 h was analyzed. The microstructural parameters, including dislocation density (δ), microstrain (ϵ), and crystallite size (D), were evaluated using the following equations.^{22,23}

$$D = (0.9\lambda)/(\beta\cos\theta), \quad (1)$$

$$\epsilon = (\beta\cos\theta)/4, \quad (2)$$

$$\delta = 1/(D^2). \quad (3)$$

Here, D represents the crystallite size, θ is the Bragg angle, β is the full width at half maximum in radians, ϵ is microstrain, λ is X-ray wavelength, and δ is dislocation density. The results show that the size of the crystallites increased with increasing film layer thickness. As the thickness of the thin film samples increases, more material becomes available for crystallite nucleation and growth, which causes the crystallite size to increase. This is because the increase in thickness results in a decrease in dislocation density and strain, which improves the quality of the thin films (the crystalline structure becomes more regular when imperfections are decreased) and consequently increases the crystallite size. Similar results (variation in crystallite size with thickness of prepared films) have been reported in the literature.^{24,25} The structural parameters of the thin films are presented in Table I.

Many reflection peaks were identified from the XRD pattern, with a high-intensity peak at 38.7° and low-intensity peaks at 32.21°, 36.14°, 44.89°, and 64.93°, associated with the (200), (110), (−111), (−112), and (−312) planes, respectively, confirmed by JCPDS card no. 05-0661. The graph shows that the crystallinity of the highest peak

increased with increasing film thickness. This suggests that slow spinning speeds resulted in good crystallinity, which is consistent with previous reports^{26,27} (Fig. 2).

Morphological Analysis

It was observed that as the thickness of the films decreased from 370 nm to 157 nm, the grain size decreased from 45 nm to 41 nm, respectively. Morphological analysis revealed that the reduction in thickness caused the decrease in grain size. These results agree well with the findings reported by Saif et al.²⁸ Figure 3 shows that the grain size obtained from SEM analysis was large in comparison with the grain size obtained from the XRD analysis.

Optical Properties

The Tauc relation was used to calculate the band gap of the synthesized films.^{29,30}

$$(\alpha hv)^2 = A (hv - E_g), \quad (4)$$

$$\alpha = \frac{1}{t} \ln\left(\frac{1}{T\%}\right). \quad (5)$$

Here, photon energy is represented by hv , the optical band gap is represented by E_g , the thickness is represented by t , and transmission is represented by T (Fig. 4).

The optical band gap was found to decrease from 2 eV for 0.75 M1 to 1.69 eV for 0.75 M3. When the film thickness increased, the band gap narrowed, indicating an improvement in the film performance. Because of the band gap range of 1.69–2 eV, these films can be utilized as gas detection elements. These findings are consistent with those of Shariffudin et al.³¹ The band gap begins to increase as

Table I Structural parameters of CuO films

Thickness (nm)	Spinning speed (rpm)	Size of crystallite D (nm)	Microstrain ϵ	Dislocation density δ (m ⁻²)
157	2500	18.14	0.0048	3.03×10^{15}
370	2000	25.09	0.00147	1.58×10^{15}
470	1500	27.48	0.00132	1.32×10^{15}

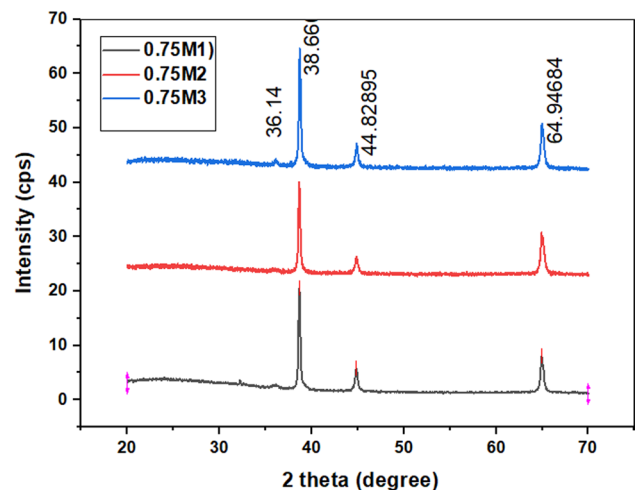


Fig. 2 XRD pattern of CuO thin film samples.

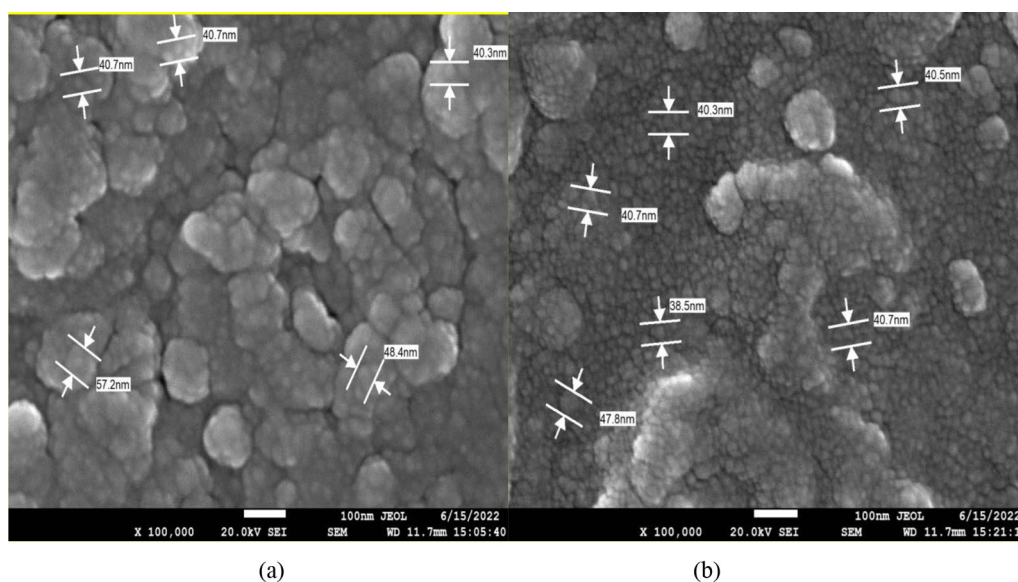


Fig. 3 FESEM images of CuO films with thickness of (a) 370 nm and (b) 157 nm.

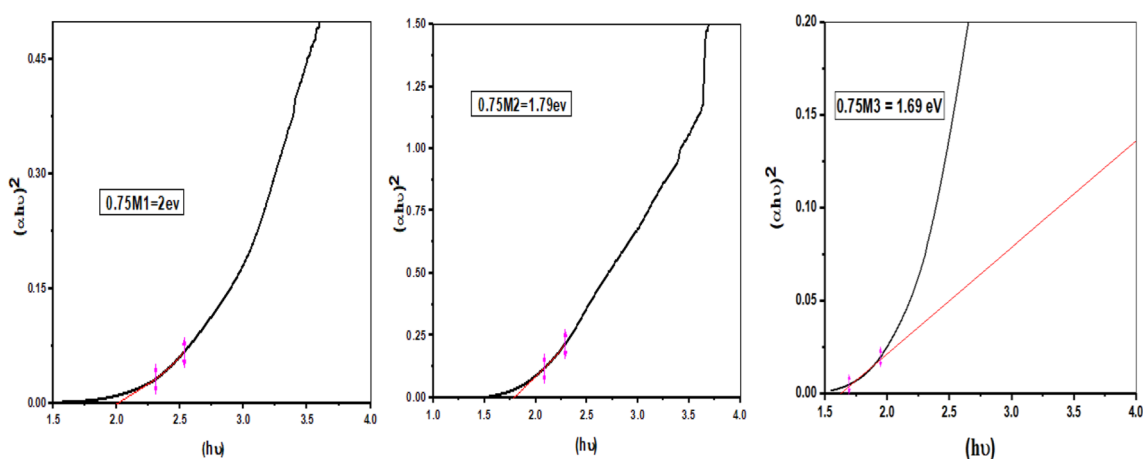


Fig. 4 Plot of band gap energy versus photon energy for samples 0.75 M1, 0.75 M2, and 0.75 M3.

film thickness decreases. This is because thinner films have higher spatial confinement, which increases the energy levels of the electrons and holes. This variation in optical band gap with thickness can have important consequences for applications involving gas sensing. Because of the increased surface area-to-volume ratio, thinner films with a large band gap may show greater sensitivity to specific gases.

Electrical Properties

Different samples with a concentration of 0.75 M and varying thickness of 157 nm, 370 nm, and 470 nm were designated as 0.75 M1, 0.75 M2, and 0.75 M3, respectively. Within the voltage range of 1–10 V, the I – V dependence was linear, demonstrating the ohmic nature of the silver

contact in the films. As shown in the graph in Fig. 5, the I – V characteristics of the prepared samples are dependent on the film thickness.

An increase in film thickness results in an increase in the number of electrons and holes (sheet resistance and conductivity), while the bulk concentration may remain the same. The electrical resistivity of the thin films was measured by a two-probe setup. The resistivity and conductivity were calculated using Eqs. 6, 7, and 8.²⁵ The CuO thin film had the lowest resistivity for the 0.75 M3 sample and the highest resistance for the 0.75 M1 sample. The decrease in resistivity occurred because of an increase in the concentration of both holes and electrons as carriers. The electrical characteristics of thin films synthesized using copper acetate dihydrate as a precursor

can be significantly impacted by the spinning speed during sol–gel spin coating. Because of the increased centrifugal force, film thickness decreases as spinning speed increases. The findings of this study demonstrate that the current was highest at a spin speed of 1500 rpm and lowest at a spin speed of 2500 rpm. Because the active region received more charge carriers, the recombination process was able to proceed successfully, producing improved electrical characteristics. As the resistivity decreased, electrical conductivity increased.³² The mechanism driving the observed increase in conductivity with increasing

thickness of CuO thin films is related to the increase in the number of charge carriers available for conduction. Thicker films provide more pathways for charge carriers to flow through, resulting in higher conductivity.

$$R = \frac{\pi}{\ln 2} \times \frac{V}{I}, \tag{6}$$

$$\rho = R \times t \tag{7}$$

where ρ is the resistivity of the thin films and t is the film thickness.

$$\sigma = \frac{1}{\rho}. \tag{8}$$

Here, V is the applied voltage, I is the acquired current, R is the mean resistance, and σ is the conductivity of the thin films (Fig. 6).

At 1500 rpm, the resistivity of 0.75 M3 was 42.51 Ω -m, while at 2500 rpm the resistivity of 0.75 M1 was 75.53 Ω -m. The reduced resistivity resulted from an increase in the concentration of electrons and holes as carriers. Consequently, the maximum resistivity was produced by CuO thin films with the fastest spin coating speed and the lowest carrier concentration.

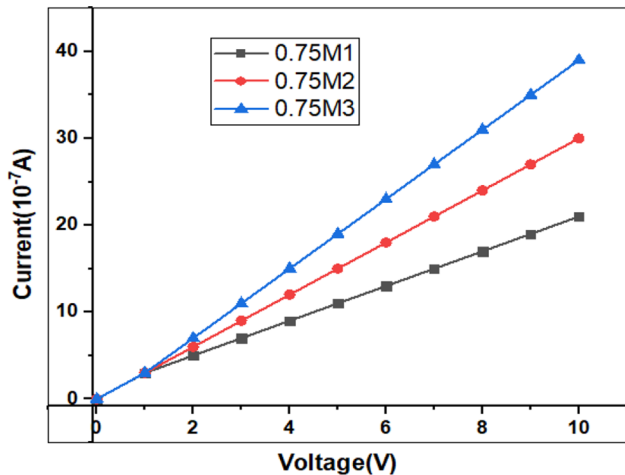


Fig. 5 I–V properties of CuO thin films.

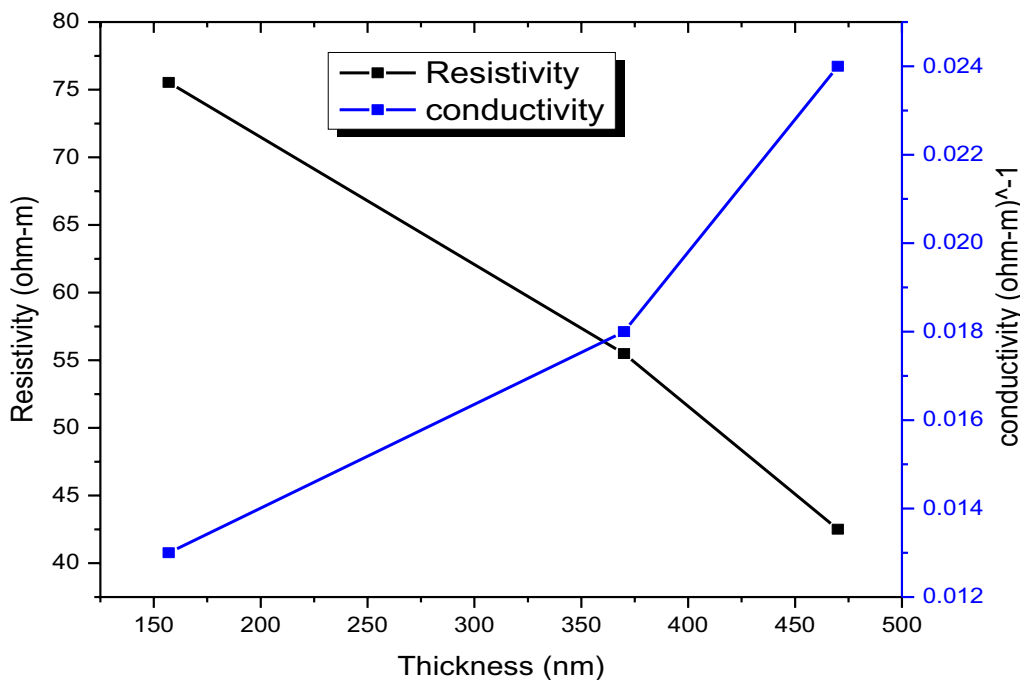


Fig. 6 Variation in resistivity and conductivity with varying film thickness.

Gas Sensing

The relative change in the signal monitored during gas exposure indicates the film's sensitivity. The formula for the gas response of the sensor is the ratio of the change in the sample's resistance when tested with target gas versus the resistance it experiences in air:

$$S = R_a/R_g. \quad (9)$$

Here, resistance in the presence of gas and air is represented by R_a and R_g , respectively.

When the sample is placed in air, molecules of oxygen are adsorbed on the surface of gas sensing elements and create O^- ions. When H_2S gas is injected on CuO thin films, it reacts with adsorbed O^- ions and forms CuS. The operating temperature significantly affects the response of semiconductor-based sensors. High temperature can enhance sensitivity by promoting chemical reactions between the gas and sensor material, but excessive heat can degrade the sensor performance or lifespan. Therefore, maintaining an optimal temperature range is crucial for reliable and accurate detection. It was observed that on exposure to H_2S gas, the response of the film also started to decrease as the operating temperature increased, which is explained by the phenomenon of oxygen desorption. This could be due to the material's reaction with H_2S , which may be less favorable at higher temperatures, decreasing the sensor's response toward gas (Fig. 7).

In order to determine the working temperature, the CuO films were exposed to 40 ppm of hydrogen sulfide at a range

of temperatures from 25°C to 150°C, as shown in Fig. 7. It is frequently reported in the literature that a standard operating temperature corresponds to the maximal response. Figure 8 shows that as the concentration of target gas was increased from 10 ppm to 40 ppm, an increase in gas response was observed. On exposure to higher concentrations of H_2S gas, the sensitivity of the prepared CuO thin films increased due to an increase in the number of carriers because of the adsorption of oxygen ions (O^- and O^{2-}) on reactive sites.³³ As the operating temperature increased, the sensitivity decreased, which is explained by the adsorption and desorption of oxygen.³⁴ Decreasing sensitivity due to increasing operating temperature is based upon desorption. At higher temperatures, H_2S molecules tend to desorb more readily from the surface of CuO thin films, reducing the number of gas molecules available for detection. This phenomenon decreases the overall sensitivity of the sensor. Synthesized thin films of CuO can be used as a gas sensor to monitor H_2S gas, because upon exposure to this gas, the prepared samples show a large change in conductivity. One commercially available device that incorporates CuO thin films for gas sensing is the MQ-136 gas sensor module. The significance of the current work is that we prepared pure CuO thin films of 0.75 M concentration which can be used as a sensing element for a gas sensor available in the market. The sensitivity of three samples was determined and found to decrease with increasing film thickness. The response and recovery time of the films was noted, with a minimum response time of 20 s and minimum recovery time of 6 min. Thinner films demonstrated higher sensitivity and faster response due to increased surface area. The decrease in grain size resulted in an increase in the surface-to-volume ratio,

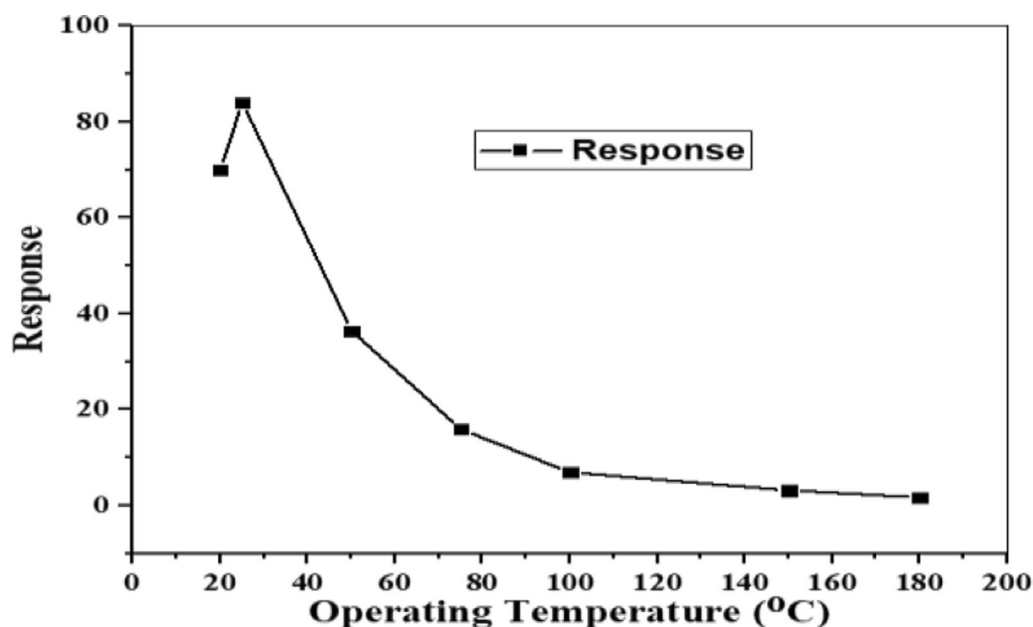


Fig. 7 Response toward H_2S gas at different temperatures.

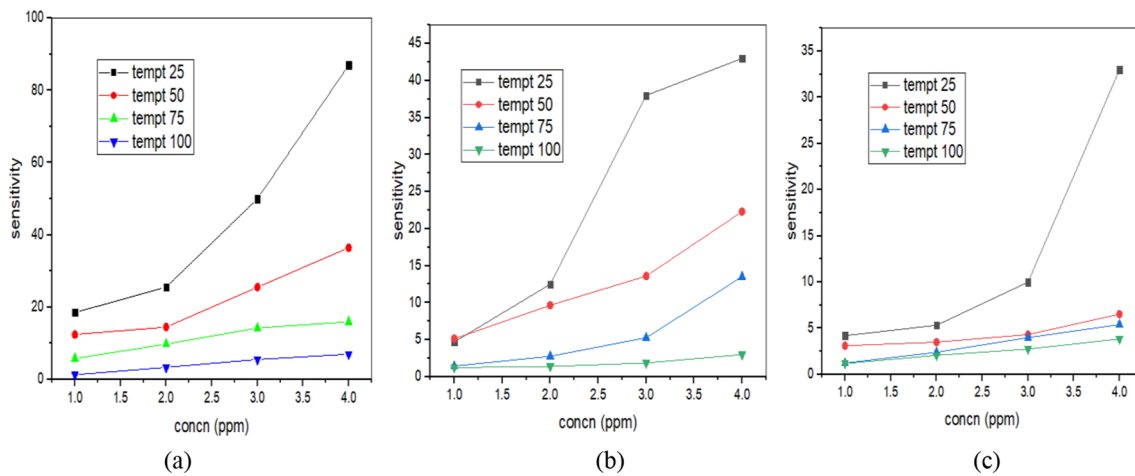


Fig. 8 Change in response on varying gas concentration and operating temperature obtained for the films with thickness of (a) 157 nm, (b) 370 nm, (c) 470 nm.

Table II Response parameters shown by sample 0.75 M1

Concentration of gas	Response parameters	Operating temperature (°C)			
		25	50	75	100
10 ppm	Sensitivity (R_a/R_g)	18.51	12.43	5.76	1.27
	R_t (s)	70	70	68	60
	Re_t (s)	180	175	168	160
20 ppm	Sensitivity (R_a/R_g)	25.55	14.5	9.76	3.35
	R_t (s)	60	60	55	52
	Re_t (s)	420	417	408	388
30 ppm	Sensitivity (R_a/R_g)	50	25.52	14.22	5.51
	R_t (s)	50	48	42	38
	Re_t (s)	480	470	450	402
40 ppm	Sensitivity (R_a/R_g)	87	36.44	15.92	6.96
	R_t (s)	20	20	18	15
	Re_t (s)	720	712	700	688

Table III Response parameters shown by sample 0.75 M2

Concentration of gas	Response parameters	Operating temperature (°C)			
		25	50	75	100
10 ppm	Sensitivity (R_a/R_g)	5.13	4.7	1.45	1.25
	R_t (s)	75	75	70	68
	Re_t (s)	180	178	170	160
20 ppm	Sensitivity (R_a/R_g)	12.5	9.66	2.77	1.4
	R_t (s)	70	60	55	52
	Re_t (s)	240	238	228	220
30 ppm	Sensitivity (R_a/R_g)	38	13.6	5.28	1.87
	R_t (s)	60	48	42	38
	Re_t (s)	300	298	290	285
40 ppm	Sensitivity (R_a/R_g)	43	22.3	13.51	3
	R_t (s)	55	20	18	15
	Re_t (s)	660	660	650	630

consequently increasing sensitivity. The results obtained were in good agreement with those reported in the literature.^{35–37}

From the observed results, it was concluded that the thinnest films exhibit faster response and recovery time due to the lower mass and diffusion distance. Tables II, III, and IV illustrate the gas parameters achieved by samples 0.75 M1 (thickness of 157 nm), 0.75 M2 (thickness of 370 nm), and 0.75 M3 (thickness of 470 nm), respectively, with varying operating temperature and gas concentration.

Conclusion

Copper oxide films were synthesized by varying the spinning speed in the range of 1500–2500 rpm. The crystallite size and crystallinity of the thin films were analyzed by XRD.

Table IV Response parameters shown by sample 0.75 M3 (470 nm).

Concentration of gas	Response parameters	Operating temperature (°C)			
		25	50	75	100
10 ppm	Sensitivity (R_a/R_g)	4.2	3.11	1.23	1.18
	R_t (s)	78	78	76	70
	Re_t (s)	120	120	110	108
20 ppm	Sensitivity (R_a/R_g)	5.33	3.5	2.4	2.07
	R_t (s)	70	60	55	52
	Re_t (s)	900	880	850	800
30 ppm	Sensitivity (R_a/R_g)	10	4.32	3.99	2.75
	R_t (s)	60	48	42	38
	Re_t (s)	1500	1498	1490	1485
40 ppm	Sensitivity (R_a/R_g)	33	6.53	5.4	3.84
	R_t (s)	55	20	18	15
	Re_t (s)	1800	1790	1650	1600

It was observed that the crystallite size increased as the thickness increased. With increased thickness, dislocation energy decreases, which shows that there is a more regular crystalline structure because of the reduction in imperfections. FESEM revealed the morphology and grain size of the films, indicating that a reduction in thickness will result in a decrease in the grain size. From the two-probe set-up, the $I-V$ characteristics were found to be ohmic in nature, and the conductivity of the films was found in the range of $0.013 \Omega^{-1} \text{ m}^{-1}$ to $0.024 \Omega^{-1} \text{ m}^{-1}$. Conductivity was found to increase with the increase in film thickness. These prepared samples were used to detect the concentration of H_2S gas. Studies showed that when gas concentration increases, so does the sensitivity. The highest sensitivity of all samples was found at room temperature.

Author Contributions Jyoti: synthesis and characterization of samples, H_2S gas analysis on samples, writing of manuscript, result analysis using software (origin). Rajesh Kumar: supervision, editing of manuscript.

Data Availability Experiments were used to collect the data, and the organization also supplied additional materials.

Conflict of interest The authors declare that they are not aware of any personal or financial conflicts that might have appeared to affect the research reported in this study.

References

- W.H. Brattain and J. Bardeen, Surface properties of germanium. *Bell Syst. Tech. J.* 32, 1 (1953).
- A. Dey, Semiconductor metal oxide gas sensors: a review. *Mat. Sci. Eng. B.* 229, 206 (2018).
- N.M. Vuong, N.D. Chinh, B.T. Huy, and Y.I. Lee, CuO-decorated ZnO hierarchical nanostructures as efficient and established sensing materials for H_2S Gas Sensors. *Sci. Rep.* 6, 26736 (2016).
- D.C. Glass, A review of health effects of hydrogen sulphide exposure. *Ann. Occup. Hyg.* 34, 323 (1990).
- S.K. Pandey, K.H. Kim, and K.T. Tang, A review of sensor-based methods for monitoring hydrogen sulfide. *TrAC - Trends Anal. Chem.* 32, 87 (2012).
- J. Zhang, S. Ma, B. Wang, and S. Pei, Hydrothermal synthesis of SnO_2 -CuO composite nanoparticles as a fast-response ethanol gas sensor. *J. Alloy. Compd.* 886, 161299 (2021).
- L.-Y. Zhu, K. Yuan, J.-G. Yang, H.-P. Ma, T. Wang, X.-M. Ji, J.-J. Feng, A. Devi, and H.-L. Lu, *Respir Res.* 20, 233 (2019).
- Y.Y. Wang, G.T. Duan, Y.D. Zhu, H.W. Zhang, Z.K. Xu, Z.F. Dai, and W.P. Cai, Room temperature H_2S gas sensing properties of In_2O_3 micro/nanostructured porous thin film and hydrolyzation-induced enhanced sensing mechanism. *Sens. Actuators B* 228, 74 (2016).
- Z. Guo, G. Chen, G. Zeng, L. Liu, and C. Zhang, Metal oxides and metal salt nanostructures for hydrogen sulfide sensing: mechanism and sensing performance. *RSC Adv.* 5, 54793 (2015).
- M.N. Hassankiadeh and A. Hallajisani, Application of molybdenum oxide nanoparticles in H_2S removal from natural gas under different operational and geometrical conditions. *J. Pet. Sci. Eng.* 190, 107131 (2020).
- J. Liu, X. Wang, Q. Peng, and Y. Li, Vanadium Pentoxide Nanobelts: highly selective and stable ethanol sensor materials. *Adv. Mater.* 17, 764–767 (2005).
- A. Yang, W. Li, J. Chu, D. Wang, H. Yuan, J. Zhu, X. Wang, and M. Rong, Enhanced sensing of sulfur hexafluoride decomposition components based on noble-metal functionalized cerium oxide. *Mater. Des.* 187, 108391 (2020).
- N.M. Hieu, D.V. Lam, T.T. Hien, N.D. Chinh, N.D. Quang, N.M. Hung, C. Van Phuoc, S.M. Lee, J.-R. Jeong, C. Kim, and D. Kim, ZnTe-coated ZnO nanorods: hydrogen sulfide nano-sensor purely controlled by p-n junction. *Mater. Des.* 191, 108628 (2020).
- K. Zhang, S. Qin, P. Tang, Y. Feng, and D. Li, Ultra-sensitive ethanol gas sensors based on nanosheet-assembled hierarchical $\text{ZnO-In}_2\text{O}_3$ heterostructures. *J. Hazard. Mater.* 391, 122191 (2020).
- J.-H. Kim, A. Mirzaei, J.H. Bang, H.W. Kim, and S.S. Kim, Selective H_2S sensing without external heat by a synergy effect in self-heated CuO-functionalized SnO_2 -ZnO coreshell nanowires. *Sens. Actu. B Chem.* 300, 126981 (2019).
- L. Yin, G. Qu, P. Guo, R. Zhang, J. Sun, and D. Chen, Construction and enhanced lowtemperature H_2S -sensing performance of novel hierarchical CuO@WO₃ nanocomposites. *J. Alloys Compd.* 785, 367 (2019).
- M.H. Raza, K. Movlaee, S.G. Leonardi, N. Barsan, G. Neri, and N. Pinna, Gas sensing of NiO-SCCNT core-shell heterostructures: optimization by radial modulation of the holeaccumulation layer. *Adv. Funct. Mater.* 30, 1906874 (2019).
- F. Mendoza, D.M. Hernández, V. Makarov, E. Febus, B.R. Weiner, and G. Morell, Room temperature gas sensor based on tin dioxide carbon nanotubes composite films. *Sens. Actu. B Chem* 190(1), 227 (2014).
- X. Hu, Z. Zhu, C. Chen, T. Wen, X. Zhao, and L. Xie, Highly sensitive H_2S gas sensors based on Pd-doped CuO nanoflowers with low operating temperature. *Sens. Actus. B: Chem.* 253, 809 (2017).
- J. Zhou, M. Ikram, A.U. Rehman, J. Wang, Y. Zhao, K. Kan, W. Zhang, F. Raziq, L. Li, and K. Shi, Highly selective detection of NH_3 and H_2S using the pristine CuO and mesoporous In_2O_3 @CuO multijunctions nanofibers at room temperature. *Sens. Actu. B Chem.* 255, 1819 (2018).
- Q. Zhao, G. Ma, C. Zhai, X. Yang, and M. Zhang, Facile synthesis of nanosheets-assembled hierarchical copper oxide microspheres and their ethanol gas sensing properties. *New J. Chem.* 41, 15042 (2017).
- Z. Essalhi, B. Hartiti, A. Lfakir, B. Mari, and P. Thevenin, Optoelectronics properties of TiO₂: Cu thin films obtained by sol gel method. *Opt. Quan. Elect.* 49, 1 (2017).
- A. Abuhasan, C. Balasingh, and P. Predecki, Residual stresses in Alumina/Silicon Carbide (Whisker) composites by X-ray diffraction. *J. Ame. Ceram. Soc.* 73(8), 2474 (1990).
- S.A.M.H.M. Ali, and S. Makki, A, The thickness effects characterization properties of copper oxide thin films prepared by thermal evaporation technique. *J. Mult. Eng. Sci. Stud.* 2, 532 (2016).
- H. Absike, H. Labrim, B. Hartiti, M. Tahri, and H. Ez-Zahraouy, Influence of spinning speed on the physical properties of sol-gel spin coated CuO films. *Mol. Cryst. Liq. Cryst.* 711(1), 18 (2020).
- H. Liang, X. Zhao, Z. Yu, M. Cao, and H. Liu, Effect of ultrasonic irradiation on structure and electrochemical properties of LiMn₂O₄ thin films cathode material for Li-ion micro-batteries. *Sol. Stat. Ion.* 192(1), 339 (2011).
- T. Balakrishnan, N.S. Subramanian, and A. Kathalingam, Studies on rheological, structural, optical, electrical and surface properties of LiMn₂O₄ thin films by varied spin rates. *Mater. Sci. Poland* 35, 626 (2017).

28. A.A. Saif, Z.A.Z. Jamal, and P. Poopalan, Influence of the grain size on the conduction mechanism of barium strontium titanate thin films. *Zeit. für Natur. A* 66(12), 784 (2011).
29. J. Tauc and A. Menth, States in the gap. *J. Non-Cryst. Solids Non-Cryst. Solids*. 8, 569 (1972).
30. S.C. Ray, Preparation of copper oxide thin film by sol-gel-like dip technique and study of their structural and optical properties. *Sol. Ene. Mat. Sol Cells* 68(3), 307 (2001).
31. S.S. Shariffudin, S.S. Khalid, N.M. Sahat, M.S.P. Sarah, and H. Hashim, Preparation and characterization of nanostructured CuO thin films using sol-gel dip coating. *IOP Conf. Series: Mater. Sci. Eng.* 99, 012007 (2015).
32. S. Visalakshi, R. Kannan, S. Valanarasu, A. Kathalingam, and S. Rajashabala, Studies on optical and electrical 289 properties of SILAR-deposited CuO thin films. *Ene. Mat.* 21(3), 146 (2016).
33. F.-N. Meng, X.-P. Di, H.-W. Dong, Y. Zhang, C.-L. Zhu, C. Li, and Y.-J. Chen, Ppb H₂S gas sensing characteristics of Cu₂O/CuO sub-microspheres at low-temperature. *Sensor. Actuator. B Chem.* 182, 197 (2013).
34. D. Jundale, S. Pawar, M. Chougule, P. Godse, S. Patil, B. Raut, S. Sen, and V. Patil, Nanocrystalline CuO thin films for H₂S monitoring: microstructural and optoelectronic characterization. *J. Sen. Techn.* 1, 36 (2011).
35. F.I.M. Ali, S.T. Mahmoud, F. Awwad, Y.E. Greish, and A.F.S. Abu-Hani, Low power consumption and fast 304 response H₂S gas sensor based on a chitosan-CuO hybrid nanocomposite thin film. *Carb. Poly.* 236, 116064 (2020).
36. Z. Haung, C. Fan, F. Sun, X. Wang, M. Majidi, P. Kumar, and B. Liu, Enhanced H₂S gas sensing properties by 306 the optimization of p-CuO/n-ZnO composite nanofibers. *J. Mater. Sci.* 55, 7702 (2020).
37. A. Kumar, A.K. Shringi, and M. Kumar, Sputtered CuO anchored SnO₂ for H₂S gas sensor. *Sens. Actua 308 B: Chem.* 370, 132417 (2022).

Publisher's Note Springer Nature remains neutral with regard to jurisdictional claims in published maps and institutional affiliations.

Springer Nature or its licensor (e.g. a society or other partner) holds exclusive rights to this article under a publishing agreement with the author(s) or other rightsholder(s); author self-archiving of the accepted manuscript version of this article is solely governed by the terms of such publishing agreement and applicable law.